Dynamic Control of Distal Spatial Mode Pattern Output From Multimode Fiber Using Integrated Coherent Network

Dan Yi [ID], *Member, IEEE*, Xuetong Zhou [ID], *Graduate Student Member, IEEE*, and Hon Ki Tsang [ID], *Fellow, IEEE*

Abstract—The mode field distribution at the distal end of a multimode fiber can vary randomly when environmental perturbations introduce changes in the relative phases of different eigenmodes and variations in coupling among modes. Random rotations of the high-order mode-field distribution at the distal end can produce large coupling losses at the multimode waveguide grating coupler (MWGC) in the fiber-chip interface. In this paper, we propose a solution to this problem by using a novel approach based on controlling the relative phases and amplitudes of different modes launched at the proximal end of the fiber. We implemented an integrated mesh of Mach Zehnder Interferometer at the transmitter to demonstrate control of the distal end mode field distribution to ensure low coupling losses in the receiver's MWGC. The MWGC on the silicon-on-insulator (SOI) platform had measured coupling efficiency of (-5.7 dB, -7.1 dB) for (LP01x, LP11ax) modes, without needing any manual adjustment to align the mode orientation with the MWGC. The coherent Mach-Zehnder Interferometer (MZI) network can be dynamically controlled to produce the desired mode pattern at the distal end of the FMF to enable low-loss coupling at the distal end. This enables the practical deployment of mode division multiplexing with MWGC without needing manual control of fiber orientation at the receiver. The proof-of-concept experiment demonstrates that the transmitter mode control is suitable for future deployment of mode division-multiplexing (MDM) data center interconnects.

Index Terms—Integrated optics, coherent network, few mode fibers, space-division multiplexing.

I. INTRODUCTION

DRIVEN by the 25∼30% compound growth rate of data traffic in recent years, there has been widespread research to increase the transmission capacity of optical fiber communications beyond the theoretical limit imposed by Shannon's information theory and nonlinear fiber effects [1], [2]. Advanced multiplexing and modulation techniques [1], [3], [4], [5], [6], time-division multiplexing [3], polarization division multiplexing (PDM) [4], space-division multiplexing [1], [6], and wavelength division-multiplexing [5] have all been well explored.

The new dimension of space-division multiplexing (SDM) can be exploited by the introduction of the use of few-mode fibers (FMFs) [7], multi-core single-mode fibers (MC-SMFs) [8], multi-core few-mode fibers (MC-FMFs) [9] or mode division multiplexing in multimode fibers [10]. Data rates exceeding 2 Pbit s^{-1} across 100 spatial channels in multimode MCFs have been demonstrated [11], [12]. FMF erbium-doped fibre amplifiers [13], [14] have also been developed for optical communications. Different types of spatial multiplexers (SMUXs) based on bulk optics [7], [15], multiplane light conversion using phase plates [10], fiber-based photonic lanterns [16], [17], [18], laser-inscribed three-dimensional waveguide devices [19], [20], and integrated photonic device [21], [22], [23], [24], [25], [26], [27], [28], [29], [30], [31], [32], [33] have been developed for the interface between multiple SMFs and the SDM fibers.

Integrated SMUXs based on silicon-on-insulator (SOI) platform have the advantages of compact footprint, high reliability, and low-cost mass-production scalability when compared with the other technologies for SMUXs. Integrated SMUXs using either edge couplers [32], [33] or vertical diffraction grating couplers [21], [22], [23], [24], [25], [26], [27], [28], [29], [30], [31] have been demonstrated with quite competitive coupling efficiencies, and coupling losses as low as 1.36 dB [30] having been demonstrated for selective coupling to two LP modes in few-mode fibers using multimode waveguide grating couplers [MWGC]. Except for efficient coupling interfaces between SMF and FMFs, the problem of high loss outage [34], [35] at the receiver, introduced by mode coupling and mode distribution rotation is a problem that needs to be addressed for deployment using integrated MWGC. For example, the desired LP modes may become rotated by environmental perturbations and introduce very high coupling losses at the receiver's fiber-chip interface. In our previous proof-of-concept demonstration of MDM in the FMF, our group employed a conventional manual three-paddle mechanical polarization controller that was adapted for use with the FMF. We used this controller to manually adjust the rotation of the mode field, aligning the modes' orientation (rather than polarization) in the polarization diversity waveguide grating coupler. [27]. But this manually-adjustable FMF-PC is not practical for use in the field, because the mode field pattern can change with environmental changes in temperature and fiber strains [36]. Therefore, an electronic dynamic controller is necessary.
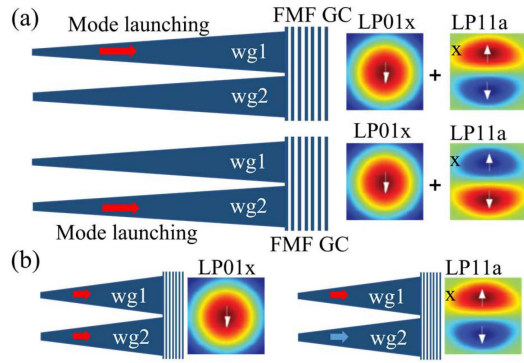
Fig. 1. Principle of the proposed mode multiplexer. (a) The field pattern of the LP01-x mode and LP11a- x mode of a FMF. If we launch the light from wg1 and wg2, a combination of LP01-x and LP11a-x will be excited from the FMF GC. (b) If we launch light from wg1 and wg2 simultaneously with the same phase, LP01-x will be excited in the FMF. If we launch light from wg1 and wg2 simultaneously but with a relative phase of π, LP11a-x will be excited in the FMF.

In this paper, we show that the MZI-based coherent network as the transmitter can be used to effectively modify the mode field distribution at the distal end of the multimode fiber. We can separate the different data channels at the far end of the few-mode fiber (FMF) even when mode crosstalk is introduced due to misalignment between the transmitter MWGC and the optical fiber transmission. By utilizing the integrated device, we demonstrate the ability to synthesize the LP01 and LP11 modes individually at the far end through control of the phase shifters in the transmitter.

II. PRINCIPLE AND DESIGN OF TRANSMITTER

A. Launching of the LP01 and LP11a Modes

The proposed mode multiplexer is based on an integrated mode multiplexer by selective launching of light to the few-mode fiber grating coupler (FMF GC) from different single-mode input waveguide as shown in Fig. 1. To excite the LP01-x mode of a FMF, equal power of light from wg1 and wg2 with zero phase difference is launched into the FMF GC. To excite the LP11a-x mode of a FMF, equal power of light from wg1 and wg2 with π phase difference needs to be launched into the FMF GC, as shown in Fig. 1(b). The vertical FMF grating couplers are designed to support the coupling of LP01-x and LP11a-x modes. By controlling the relative ratio and phases of the two paths (wg1 and wg2), arbitrary combination of (LP01-x, LP11a-x) modes in the FMF can be launched.

B. Design of Vertical FMF GC

The fabricated FMF GC is designed for an FMF with a core diameter of 19.5 μm. Fig. 2(a) and (b) show its working principle, i.e., LP01-x and LP11a-x modes are launched into TE0 and TE11 modes of the multi-mode waveguide, respectively. The genetic optimization method was used to optimize the grating periods of the grating. The FMF-GC used here is shallow etched as illustrated in Fig. 2(a) and (b). Design simulation results indicate coupling efficiency of (−4.8 dB, −6.81 dB) at 1560.0
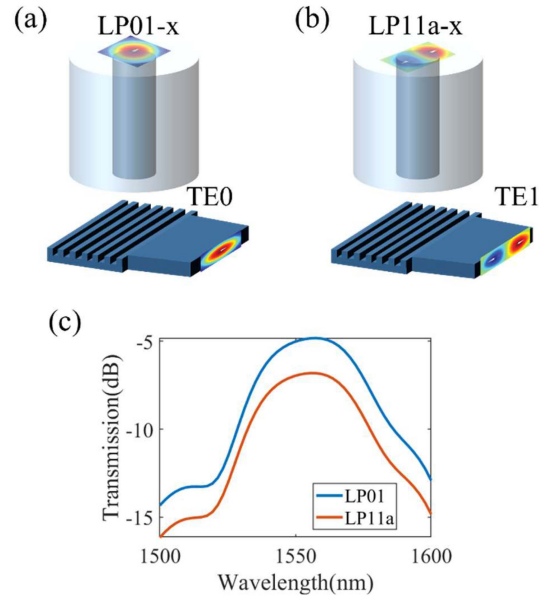

Fig. 2. Principle of the FMF mode multiplexer. (a) LP01-x will be launched into TE0 mode of the waveguide. (b) LP11-x mode will be launched into TE1 mode of the waveguide. (c) The simulated coupling efficiency of the designed FMF GC.

nm for (LP01−x, LP11a−x) mode which is different from Ref. [27] because the device fabrication parameters and process development kit (PDK) are different due to the use of a different foundry. The 3-dB bandwidth of the simulation results for both channels is 43 nm. The insertion loss can be further reduced by an overlay of poly-Si layer [30].

C. Theory for the Mode Synthesizer

The intensity pattern at the distal end of the FMF is sensitive to changes in the precise positioning of the FMF relative to the FMF GC, tuning of the optical wavelength of the input laser, physical rotation state of the FMFs, and the presence of random strain-induced changes of the relative phases of different eigenmodes of the FMF. To estimate the power in unwanted mode in the FMF, we constructed the following model: The transmission matrix between two input waveguides [wg1, wg2]^T and the received eigenmodes [LP01, LP11]^T at the distal end of the FMF can be described by [S11, S12; S21, S22]. If the FMF is aligned well with the FMF GC, and there is no mode crosstalk in the FMF, the transmission matrix is $\frac{a}{b}\begin{bmatrix} 1 & 1 \\ 1 & -1 \end{bmatrix}$. The value of a and b may be different if mode dependent loss is introduced by the FMF GC. When the FMF is displaced by a small distance from the optimum position relative to the waveguide grating coupler, mode crosstalk is introduced, and the transmission matrix becomes $\begin{bmatrix} a1 & a2 \\ b1 & b2 \end{bmatrix}$, where a_j, b_j are complex numbers. However, by controlling the phases in the MZI mesh at the transmitter, we can always tune the relative amplitude (H1) and phase difference (H2) between two input waveguides by adjusting the phase shifters to ensure the optical field in the two input waveguides (wg1, wg2) was [u1, u2]^T, where u1, u2 are also complex numbers. Only LP11 modes will be injected in the
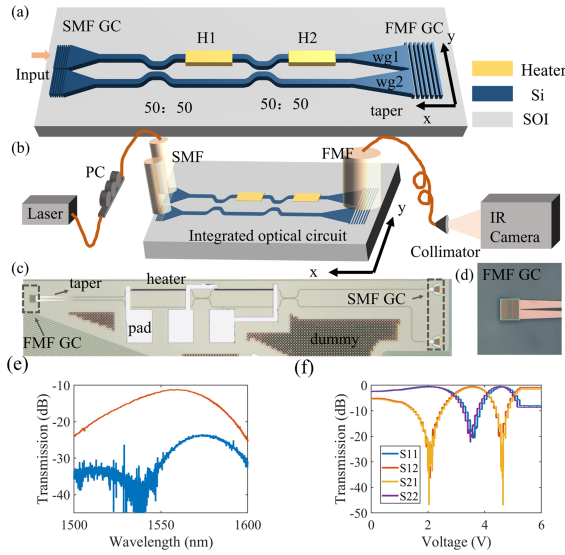
Fig. 3. (a) Schematic of the proposed system for FMF modes launching. (b) Schematic of the experimental setup. The laser we use is Santec tsl-510 and the IR camera is micron viewer 7290A. (c) Micrograph image of the fabricated device. PC represents the polarization controller. (d) Micro-graph image of the fabricated FMF GC. (e) Transmission of MZI with relationship to the applied voltage on the phase shifter. (f) Transmission spectra of the MZI when the transmission was optimized or minimized.
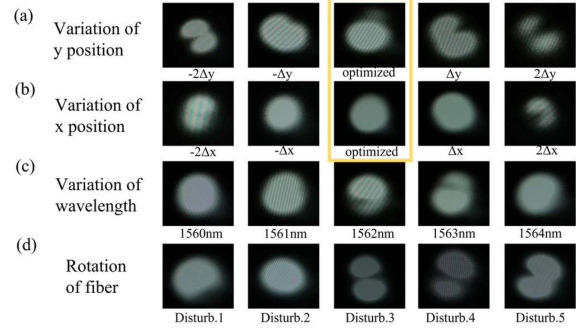

Fig. 4. Measured intensity profiles at the output of FMF when the FMF was misaligned relative to the FMF-GC along (a) y direction and (b) x direction. Figures in yellow box show the intensity patterns when the coupling was optimized in (a) y direction and (b) x direction. Measured intensity profiles at the output of a FMF when (c) we change the injection wavelength of the input laser from 1560 nm to 1564 nm with the step size of 1 nm and (d) when applying different disturbances on the short FMF.

fiber when a1u1 + a2u2 = 0 and only LP01 mode will appear in the fiber if b1u1 + b2u2 = 0. We also gave an example to show the theory can work for N > 2, such as N = 4. To inject only one mode, we need to achieve: $\begin{bmatrix} m1 \\ 0 \\ 0 \\ 0 \end{bmatrix} = \begin{bmatrix} c11 & c12 & c13 & c14 \\ c21 & c22 & c23 & c24 \\ c31 & c32 & c33 & c34 \\ c41 & c42 & c43 & c44 \end{bmatrix} \begin{bmatrix} x1 \\ x2 \\ x3 \\ x4 \end{bmatrix}$, and we can always find the solution of unit vector [x1, x2, x3, x4]^T which can be realized by the unitary MZI network.

III. DEVICE FABRICATION AND EXPERIMENTAL RESULTS

A. Device and Experimental Setup

Fig. 3(a) shows the schematic of the designed circuit. The light was launched to the input upper waveguide and was split into two waveguides (wg1 and wg2) through a MZI, which can realize U(2) unitary operation. The MZI unit contains two thermally tunable phase shifters H1 and H2. H1 was used to tune the relative power ratio between wg1 and wg2, while H2 was used to adjust their relative phase difference. Wg1 and wg2 will excite both LP01 and LP11 modes through the FMF GC. If the FMF GC is aligned well with the vertical FMF, i.e., in the middle of the FMF, light coupled into the FMF will have the same weight for wg1 and wg2. Fig. 3(b) shows the experimental setup. Continuous wave (CW) laser light at 1560 nm was launched to one of the inputs using regular single mode fiber. The output light was coupled vertically to a cleaved FMF through the FMF GC. An angled physical contact (APC) fiber connector was present at the distal end. The field profiles at the APC facet were imaged by an infrared (IR) camera after going through a collimator. Fig. 3(c) shows micrograph image of the fabricated device. The device was fabricated by a commercial foundry on a SOI wafer with standard top silicon thickness of 220 nm and

buried silicon dioxide of 2 μm. Fig. 3(d) shows the fabricated FMF GC with size of 15 μm $\times$ 18 μm which is designed to support the coupling of LP01-x and LP11a-x modes. We first characterize the performance of the MZI. The spectra of the MZI are plotted in Fig. 3(e) when the optical power was maximized or minimized at 1560 nm. The IL of the MZI is quite low and the extinction ratio (ER) is about 20 dB as also indicated by Fig. 3(f).

The optical intensity profiles at the APC facet were imaged by an infrared camera, as shown in Fig. 4(a)–(d). Except for the phase errors that exist between different waveguides, the field profile outputs from the FMF are also sensitive to many other reasons including the position deviations from the designed coupling point, optical wavelength from the input laser, and the rotation state of the FMFs. We observed these phenomena during experiments. It can be observed from Fig. 4(a) and (b) that the relative coupling of LP11a mode and LP01 mode varied significantly if the position of FMF was displaced from the optimum designed coupling point. The optical intensity distribution at the distal end is especially sensitive to the position variations along y direction. We can also observe from Fig. 4(c) that the intensity distribution is wavelength-dependent which suggests there exists mode interference in the FMF. The wavelength-dependent phase differences between LP01 and LP11 modes give rise to the wavelength-dependent intensity pattern. And if we manually add disturbance on the FMF, the intensity field will also change as illustrated in Fig. 4(d). Based on the above circumstances, it is difficult to precisely determine the optimum launch location because mode crosstalk in the FMF is also present.

B. Mode Suppression

Here we show that the coherent MZI unit can be used to compensate for mode crosstalk during coupling and transmission to help us generate desired modes at the distal end of FMF. We gave three experimental demonstrations. In the first demonstration, we manually adjusted the fiber coupling position along y direction and get the random intensity profile as shown in Fig. 5(a1) and (b1). In our system, the ER of the fabricated MZI is about 20 dB. This indicates that when the value of 0.1

Fig. 5. Measured intensity profiles at the output of FMF with fiber deviation (a1-b3), wavelength change(c1-d3), and random fiber rotations (e1-f3). The simulation results also estimate the relative percentage (pct) values of the (LP01, LP11a, and LP11b) modes. (a1) and (b1) show the intensity profile when the voltage applied on the heaters (H1, H2) to be (0, 0) V. (a2) and (b2) show the intensity profile when the injected modes were optimized to be LP11 mode. (a3) and (b3) show the intensity profile when the injected mode was optimized to be LP01 mode.

< |a1/a2| < 10 (or the uncertainty of position was limited to ± 2.1 μm), the MZI can be used to suppress the undesired modes in the FMF. It can be observed from Fig. 5 that LP11 mode group (Fig. 5(a2) & (b2)) and LP01 mode (Fig. 5(a3) & (b3)) can be excited independently if we optimize the applied voltages on (H1, H2) properly. We also utilized simulations to estimate the distribution of each eigenmode present within the FMF. For instance, in Fig. 5(a1), the initial intensity pattern consists of 55% LP01 mode and 45% LP11a mode. By optimizing the applied voltages on the phase shifters, the composition of the LP01 mode can be reduced to 5%, as shown in Fig. 5(a2), while the presence of the LP11 mode can be suppressed to 2%, as indicated in Fig. 5(a3). In the second demonstration, the fiber position was fixed but we changed the wavelength of the input laser. The intensity profiles are shown in Fig. 5(c1)–(d3). In the third demonstration, we fix both the wavelength and the fiber
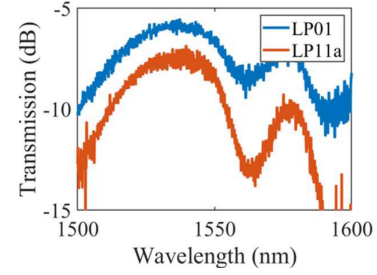

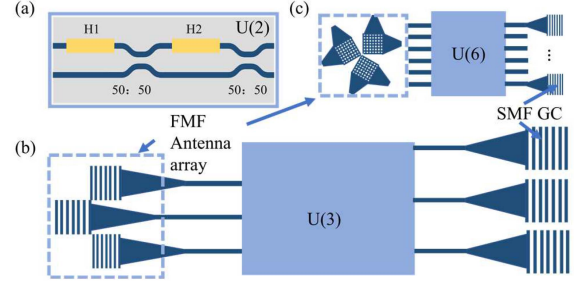Fig. 6. Measure IL of the FMF GC for LP01-x and LP11a-x modes.

Fig. 7. (a) Schematic of coherent MZI network with unitary transformation U(2). (b) Schematic of the system when we scale the number of supported modes to be 3, i.e., LP01, LP11a, and LP11b modes. (c) Schematic of the system when we scale the number of supported modes to be 6, i.e., LP01x, LP11ax, LP11bx, LP01y, LP11ay, and LP11by.

position, but the transmission fiber was rotated and perturbed with micro-bends, leading to the various received intensity patterns shown in Fig. 5(e1)–(f3). For all three cases, LP01 and LP11 modes can be synthesized separately with optimum control of (H1, H2). In this proof-of-concept demonstration, we only showed the use of two modes, LP01-x and LP11a-x mode. There was unavoidable mode crosstalk between LP11a and LP11b modes which can be observed in Fig. 5(b2), (e2), and (f2). This problem can be solved by scaling up the number of supported modes and injection waveguides of the system. The measured IL (Fig. 6) for LP01-x and LP11a-x are −5.7 dB and −7.1 dB, respectively. The 3-dB bandwidth is about 40 nm for both modes which matches with the simulation results.

C. Scaling to More Modes

The proposed structure can support more modes. Due to the limitation of the FMF GC, the current system can only support LP01 and LP11a modes. LP11b mode cannot be eliminated by optimizing two heaters. If we want to eliminate the LP11b mode in the system, it is necessary to launch 3 modes. Here we give an example using the antenna for illustration as shown in Fig. 7(b). With the U(3) unitary network, we would be able to inject LP01, LP11a, and LP11b into FMF independently. The system can be further scaled up to 6 modes using LP01, LP11a, and LP11b with dual polarization via 2D antenna array as indicated in Fig. 7(c). The U(3) and U(6) illustrated in Fig. 7 can be implemented using the MZI network configured in Ref. [37]. It is also possible to use OM4 fiber and more couplers to further scale up the supported mode channels in the system using the same theory.

IV. Conclusion

A general integrated optical circuit for controlling the intensity profile at the distal end of FMF has been proposed. Our approach was based on the use of a coherent MZI mesh to tune the relative amplitude and phase between launching waveguides. The system can selectively launch the LP01-x and LP11a-x modes despite the presence of small misalignments between the fiber and the FMF GC, or the introduction of fiber twisting or micro-bends. We implemented the optical circuit on the silicon-integrated photonics platform. Detailed test results for the device were presented in this letter. The structure can be scaled up to N modes when a multimode grating coupler is used to launch N different modes.

Acknowledgment

References

[1] D. J. Richardson, J. M. Fini, and L. E. Nelson, "Space-division multiplexing in optical fibres," *Nature Photon.*, vol. 7, no. 5, pp. 354–362, 2013.

[2] P. J. Winzer, "Making spatial multiplexing a reality," *Nature Photon.*, vol. 8, no. 5, pp. 345–348, 2014.

[3] J. Zhang and J. Yu, "Generation and transmission of high symbol rate single carrier electronically time-division multiplexing signals," *IEEE Photon. J.*, vol. 8, no. 2, Apr. 2016, Art. no. 7902506.

[4] A. Matsushita, M. Nakamura, F. Hamaoka, S. Okamoto, and Y. Kisaka, "High-spectral-efficiency 600-Gbps/carrier transmission using PDM-256QAM format," *J. Lightw. Technol.*, vol. 37, no. 2, pp. 470–476, Jan. 2019.

[5] F. Hamaoka et al., "Ultra-wideband WDM transmission in S-, C-, and L-bands using signal power optimization scheme," *J. Lightw. Technol.*, vol. 37, no. 8, pp. 1764–1771, Apr. 2019.

[6] Y. Liu et al., "Arbitrarily routed mode-division multiplexed photonic circuits for dense integration," *Nature Commun.*, vol. 10, no. 1, 2019, Art. no. 3263.

[7] R. Ryf et al., "Mode-division multiplexing over 96 km of few-mode fiber using coherent 6 × 6 MIMO processing," *J. Lightw. Technol.*, vol. 30, no. 4, pp. 521–531, Feb. 2012.

[8] K. Saitoh and S. Matsuo, "Multicore fiber technology," *J. Lightw. Technol.*, vol. 34, no. 1, pp. 55–66, Jan. 2016.

[9] Y. Sasaki, K. Takenaga, N. Guan, S. Matsuo, K. Saitoh, and M. Koshiba, "Large-effective-area uncoupled few-mode multi-core fiber," *Opt. Exp.*, vol. 20, no. 26, pp. B77–B84, Dec. 2012.

[10] G. Rademacher et al., "Peta-bit-per-second optical communications system using a standard cladding diameter 15-mode fiber," *Nature Commun.*, vol. 12, no. 1, 2021, Art. no. 4238.

[11] K. Igarashi et al., "Ultra-dense spatial-division-multiplexed optical fiber transmission over 6-mode 19-core fibers," *Opt Exp.*, vol. 24, no. 10, pp. 10213–10231, May 2016.

[12] J. Sakaguchi et al., "Large spatial channel (36-Core × 3 mode) heterogeneous few-mode multicore fiber," *J. Lightw. Technol.*, vol. 34, no. 1, pp. 93–103, Jan. 2016.

[13] E. Ip et al., "146λ × 6 × 19-gbaud wavelength-and mode-division multiplexed transmission over 10 × 50-km spans of few-mode fiber with a gain-equalized few-mode EDFA," *J. Lightw. Technol.*, vol. 32, no. 4, pp. 790–797, Feb. 2014.

[14] H. Chen et al., "Integrated cladding-pumped multicore few-mode erbium-doped fibre amplifier for space-division-multiplexed communications," *Nature Photon.*, vol. 10, no. 8, pp. 529–533, 2016.

[15] C. Koebele et al., "Two mode transmission at 2x100 Gb/s, over 40 km-long prototype few-mode fiber, using LCOS-based programmable mode multiplexer and demultiplexer," *Opt. Exp.*, vol. 19, no. 17, pp. 16593–16600, Aug. 2011.

[16] I. P. Giles, R. Chen, and V. Garcia-Munoz, "Fiber based multiplexing and demultiplexing devices for few mode fiber space division multiplexed communications," in *Proc. Opt. Fiber Commun. Conf.*, 2014, Art. no. Tu3D.1.

[17] N. K. Fontaine, R. Ryf, J. Bland-Hawthorn, and S. G. Leon-Saval, "Geometric requirements for photonic lanterns in space division multiplexing," *Opt. Exp.*, vol. 20, no. 24, pp. 27123–27132, Nov. 2012.

[18] S. G. Leon-Saval, N. K. Fontaine, J. R. Salazar-Gil, B. Ercan, R. Ryf, and J. Bland-Hawthorn, "Mode-selective photonic lanterns for space-division multiplexing," *Opt. Exp.*, vol. 22, no. 1, pp. 1036–1044, Jan. 2014.

[19] N. K. Fontaine and R. Ryf, "Characterization of mode-dependent loss of laser inscribed photonic lanterns for space division multiplexing systems," in *Proc. 18th Optoelectron. Commun. Conf. Int. Conf. Photon. Switching*, 2013, Paper MR2_2.

[20] S. Gross and M. J. Withford, "Ultrafast-laser-inscribed 3D integrated photonics: Challenges and emerging applications," *Nanophotonics*, vol. 4, no. 3, pp. 332–352, Oct. 2015.

[21] A. M. J. Koonen, C. Haoshuo, H. P. A. van den Boom, and O. Raz, "Silicon photonic integrated mode multiplexer and demultiplexer," *IEEE Photon. Technol. Lett.*, vol. 24, no. 21, pp. 1961–1964, Nov. 2012.

[22] Y. Ding, H. Ou, J. Xu, and C. Peucheret, "Silicon photonic integrated circuit mode multiplexer," *IEEE Photon. Technol. Lett.*, vol. 25, no. 7, pp. 648–651, Apr. 2013.

[23] B. Wohlfeil, G. Rademacher, C. Stamatiadis, K. Voigt, L. Zimmermann, and K. Petermann, "A two-dimensional fiber grating coupler on SOI for mode division multiplexing," *IEEE Photon. Technol. Lett.*, vol. 28, no. 11, pp. 1241–1244, Jun. 2016.

[24] T. Watanabe, M. Ayata, U. Koch, Y. Fedoryshyn, and J. Leuthold, "Perpendicular grating coupler based on a blazed antiback-reflection structure," *J. Lightw. Technol.*, vol. 35, no. 21, pp. 4663–4669, Nov. 2017.

[25] D. Garcia-Rodriguez, J. L. Corral, A. Griol, and R. Llorente, "Bimodal grating coupler design on SOI technology for mode division multiplexing at 1550 nm," *Opt Exp.*, vol. 26, no. 15, pp. 19445–19455, Jul. 2018.

[26] Y. Lai, Y. Yu, S. Fu, J. Xu, P. P. Shum, and X. Zhang, "Compact double-part grating coupler for higher-order mode coupling," *Opt. Lett.*, vol. 43, no. 13, pp. 3172–3175, Jul. 2018.

[27] Y. Tong, W. Zhou, X. Wu, and H. K. Tsang, "Efficient mode multiplexer for few-mode fibers using integrated silicon-on-insulator waveguide grating coupler," *IEEE J. Quantum Electron.*, vol. 56, no. 1, Feb. 2020, Art. no. 8400107.

[28] T. Watanabe, B. I. Bitachon, Y. Fedoryshyn, B. Baeuerle, P. Ma, and J. Leuthold, "Coherent few mode demultiplexer realized as a 2D grating coupler array in silicon," *Opt. Exp.*, vol. 28, no. 24, pp. 36009–36019, Nov. 2020.

[29] J. L. Pita Ruiz et al., "Efficient integrated tri-modal coupler for few-mode fibers," *Opt. Exp.*, vol. 30, no. 2, pp. 2539–2546, Jan. 2022.

[30] X. T. Zhou and H. K. Tsang, "High efficiency multimode waveguide grating coupler for few-mode fibers," *IEEE Photon. J.*, vol. 14, no. 4, Aug. 2022, Art. no. 6643405.

[31] C. R. Doerr, N. K. Fontaine, M. Hirano, T. Sasaki, L. L. Buhl, and P. J. Winzer, "Silicon photonic integrated circuit for coupling to a ring-core multimode fiber for space-division multiplexing," in *Proc. 37th Eur. Conf. Exhib. Opt. Commun.*, 2011, pp. 1–3.

[32] D. Melati, A. Alippi, and A. Melloni, "Reconfigurable photonic integrated mode (de)multiplexer for SDM fiber transmission," *Opt. Exp.*, vol. 24, no. 12, pp. 12625–12634, Jun. 2016.

[33] Y. Lai, Y. Yu, S. Fu, J. Xu, P. P. Shum, and X. Zhang, "Efficient spot size converter for higher-order mode fiber-chip coupling," *Opt. Lett.*, vol. 42, no. 18, pp. 3702–3705, Sep. 2017.

[34] P. J. Winzer and G. J. Foschini, "Outage calculations for spatially multiplexed fiber links," in *Proc. Opt. Fiber Commun. Conf. Expo. Nat. Fiber Optic Engineers Conf.*, 2011, pp. 1–3.

[35] P. J. Winzer and G. J. Foschini, "MIMO capacities and outage probabilities in spatially multiplexed optical transport systems," *Opt. Exp.*, vol. 19, no. 17, pp. 16680–16696, Aug. 2011.

[36] A. Li, Y. Wang, Q. Hu, and W. Shieh, "Few-mode fiber based optical sensors," *Opt. Exp.*, vol. 23, no. 2, pp. 1139–1150, 2015.

[37] W. R. Clements, P. C. Humphreys, B. J. Metcalf, W. S. Kolthammer, and I. A. Walsmley, "Optimal design for universal multiport interferometers," *Optica*, vol. 3, no. 12, pp. 1460–1465, 2016.